https://doi.org/10.5607/en23005
Exp Neurobiol. 2023 Jun;32(3):157-169.
pISSN 1226-2560 • eISSN 2093-8144

Original Article

Experimental Neurobiology

Modeling Long-term Spike Frequency Adaptation in SA-I Afferent Neurons Using an Izhikevich-based Biological Neuron Model

Jaehun Kim[1], Young In Choi[2], Jeong-woo Sohn[3*], Sung-Phil Kim[1*] and Sung Jun Jung[2*]
[1]Department of Biomedical Engineering, Ulsan National Institute of Science and Technology, Ulsan 44919,
[2]Department of Biomedical Science, Graduate School of Biomedical Science and Engineering, Hanyang University, Seoul 04763,
[3]Department of Medical Science, Catholic Kwandong University, Gangneung 25601, Korea

To develop a biomimetic artificial tactile sensing system capable of detecting sustained mechanical touch, we propose a novel biological neuron model (BNM) for slowly adapting type I (SA-I) afferent neurons. The proposed BNM is designed by modifying the Izhikevich model to incorporate long-term spike frequency adaptation. Adjusting the parameters renders the Izhikevich model describing various neuronal firing patterns. We also search for optimal parameter values for the proposed BNM to describe firing patterns of biological SA-I afferent neurons in response to sustained pressure longer than 1-second. We obtain the firing data of SA-I afferent neurons for six different mechanical pressure ranging from 0.1 mN to 300 mN from the ex-vivo experiment on SA-I afferent neurons in rodents. Upon finding the optimal parameters, we generate spike trains using the proposed BNM and compare the resulting spike trains to those of biological SA-I afferent neurons using the spike distance metrics. We verify that the proposed BNM can generate spike trains showing long-term adaptation, which is not achievable by other conventional models. Our new model may offer an essential function to artificial tactile sensing technology to perceive sustained mechanical touch.

Key words: Touch, Physiological adaptation, Afferent neuron, Neurological models, Computer simulation

INTRODUCTION

Artificial tactile sensing technology aims to replicate the human tactile sensing ability, providing humans or robots with a sense of touch [1]. Due to rapid advances in e-skin technology, the importance and viability of artificial tactile sensing technology have recently attracted much attention [2-16]. In addition, artificial tactile sensing technology has seen growing opportunities for applications in robotics and prosthetics [6, 7, 16-19].

Submitted January 18, 2023, Revised April 5, 2023,
Accepted May 19, 2023

*To whom correspondence should be addressed.
Jeong-woo Sohn, TEL: 82-32-280-6523, FAX: 82-32-280-6510
e-mail: jsohn@cku.ac.kr
Sung-Phil Kim, TEL: 82-52-217-2727, FAX: 82-52-217-2708
e-mail: spkim@unist.ac.kr
Sung Jun Jung, TEL: 82-2-2220-0612, FAX: 82-2-2220-2422
e-mail: eurijj@hanyang.ac.kr

Artificial tactile sensing technology primarily consists of e-skin, signal transmission, and tactile recognition [20, 21]. As much of this technology resembles biological tactile sensory systems, including the primary cutaneous mechanoreceptors, sensory afferent nerves, and central nervous system [22], numerous studies have taken biomimetic approaches to develop artificial tactile sensing technology [8, 23]. Inspired by neural information transmission mechanisms, biomimetic artificial tactile sensing technology capitalizes on the advantage of enabling efficient information processing with relatively low power consumption [24]. In addition to technological advances, biomimetic systems also offer opportunities to comprehend the mechanisms of biological tactile nervous systems [25].

In the biological somatosensory system, mechanical stimuli on cutaneous mechanoreceptors are transformed into action potentials and transferred to the central nervous system via tactile sensory afferents, subserving tactile perception [26]. Cutaneous tactile afferents delivering mechanical sensations are classified as slowly

adapting (SA) and rapidly adapting (RA) types. Among them, the slowly adapting type 1 (SA-I) afferent neurons transmit and encode continuous pressure and are responsible for the perception of skin shape and texture [6, 27, 28]. Hence, understanding the properties of the SA-I afferent neurons is fundamental to developing artificial tactile sensing technology. Furthermore, by mimicking the biological somatosensory system, studies that replicate the firing patterns of the SA-1 afferent have demonstrated the efficiency and performance of tactile information processing [29].

One of the ways to create the SA-I afferent neuron in artificial tactile sensing technology is to employ the biological neuron model (BNM), first established by Hodgkin and Huxley in 1952 [30], as a biomimetic approach for simulating the firing activity of a neuron by mathematically computing its membrane potential. BNM, such as the Hodgkin-Huxley model and the leaky-integrate-and-fire (LIF) model, have been used to reproduce the firing pattern of the SA-I afferent neurons [31]. Izhikevich further developed a more advanced BNM to reproduce various firing patterns [32], incorporating the advantages of both the LIF model's computational simplicity and the Hodgkin model's ability to describe various neuro-computational properties [33]. The Izhikevich spike neuron model has been widely utilized to represent the dynamics of diverse neuron types [34]. The firing patterns of the SA-I afferent neurons have also been modeled based on the Izhikevich model [35].

When modeling firings of the SA-I afferent neurons, spike frequency adaptation (SFA) with a wide range of time-constant should be considered [36]. Current BNMs implement spike frequency adaptation by determining the decay rate of spike frequency with various modeling approaches, including the power law [37] or exponential functions [38]. These models have successfully reproduced short-term adaptations of the firing rates of the SA-I afferent neurons within a few tens to hundreds of milliseconds [39].

However, it is also necessary to simulate the long-term spike frequency adaptation of the SA-I afferents that sustains much more prolonged than 1-second, which the current BNMs have not proven to achieve yet [40]. By taking a biomimetic approach and leveraging the long-term spike data in the SA-I afferent neurons, we aim to develop a novel BNM to describe the long-term spike frequency adaptation.

In this study, we propose a BNM that modifies the Izhikevich model to enable the featuring of the long-term spike frequency adaptation of the SA-I afferent in response to pressure stimulation lasting tens of seconds. To develop a new BNM, we analyze the spike train data of the SA-I afferent neurons collected from the cutaneous nerves of the mouse through ex-vivo experiments. We implement long-term spike frequency adaptation by controlling parameters that inhibit membrane recovery in the Izhikevich model depending upon the continuous firing of the SA-1 afferent, which leads to a gradual increase in interspike intervals. This new BNM generates firing patterns much closer to biological SA-1 afferent neurons than conventional models do.

MATERIALS AND METHODS

Overview of animal experiments

All experiments were conducted according to the guidelines of the Animal and Plant Quarantine Agency of Korea for the care and use of laboratory animals, and the present study was approved by the Institutional Animal Care and Use Committee of Hanyang University (HY-IACUC-13-037A). Male C57BL/6 mice (8-week-old) were used throughout the study. Ex-vivo recordings of A-fibers from a group of mice were made to examine the response of single tactile A-fibers to mechanical stimuli. The average conduction velocity of the fibers in the experiment was (32±5.2) m/s.

Animals and surgical procedure

The number of animals used throughout the study was n=6 for mechanical pressure, where one or more A-fibers were recorded from each mouse. Before surgery, mice were sacrificed by CO2 inhalation, followed by cervical dislocation. The hair on the posterior leg was shaved, and the foot was fixed on a linen pad. The hairy epidermis of the hind paw innervated by the saphenous or sural nerve was dissected after the hair on the leg was clipped. Attached connective tissue, muscle, and tendon were removed.

Setup for spike data acquisition

We placed an organ bath on an anti-vibration table containing a binocular microscope (Olympus Co., Tokyo, Japan). Light guides from the fiber-optic light source (Dolan-Jenner, Dayton, USA) were adjusted to brighten the preparation and the nerve. The spikes evoked from the tactile A-fiber were recorded with a differential amplifier (DP 311, Warner Instruments, Hamden, USA; bandpass filter: 0.1 kHz~3 kHz, gain: 10,000). Pure gold wire electrodes were plugged into the cathode and anode of the head stage of the amplifier.

The organ bath, consisting of two chambers separated by an acrylic-based wall, was perfused with warm synthetic interstitial fluid (SIF; NaCl 107.8 mM, KCl 3.5 mM, MgSO4·7H2O 0.69 mM, NaHCO3 26.2 mM, NaH2PO4·2H2O 1.67 mM, gluconic acid sodium salt 9.64 mM, glucose 5.55 mM, sucrose 7.6 mM, and CaCl2 1.53 mM saturated with a mixture of 95% O2 and 5% CO2). The heated SIF was continuously supplied to the chamber at a speed that maintained a temperature of 30~32℃.

https://doi.org/10.5607/en23005

Ex-vivo single fiber recordings

We mounted the skin-nerve preparation with the dermis side up and pinned it in the main chamber on a surface coated with poly dimethyl siloxane. The nerves attached to the skin were drawn through a tiny hole to the smaller second chamber, which was filled with paraffin oil. The nerve was placed on a fixed mirror, the sheath was removed, and nerve filaments were repeatedly teased apart to allow single-fiber recordings to be made using gold electrodes.

Signals from single tactile A-fibers were recorded extracellularly with the aforementioned amplifier. Amplified signals were sent to an oscilloscope and an audio monitor, sampled at 33 kHz, and then transferred to a computer via a data acquisition system (DAP5200a; Microstar Laboratories, Inc., Bellevue, WA, USA). Using the window discrimination feature of the software (Dapsys 8; Bethel University, http://dapsys.net/ St. Paul, MN, USA), we selectively analyzed the action potentials with the same waveform from every single fiber. Copper blocks served as a current reservoir and were connected to a common ground to prevent noise.

The conduction velocity of the axon was determined by monopolar electrical stimulation through a low-impedance electrode (CBJPL75; FHC Inc.). The supramaximal square-wave pulses (0.2 ms to 2 ms duration, 0.5 Hz) were delivered at the mechanosensitive site of a receptive field using an electrical stimulator (SD9; Grass Technologies). The distance between the receptive field and the recording electrode (conduction distance) was divided by the latency of the action potential. A single A-fiber was selected based on the conduction velocity (faster than 20 m/s); slow-conducting C-fibers were excluded. The primary search strategy was mechanical stimulation by a fire-polished glass rod targeting mechanosensitive fibers.

Identification of single A-fibers

The epineurium and perineurium of the nerve were rolled up, and the nerve bundle was teased into thin strands. We attached each strand to the cathode and pressed the skin lightly with a blunt-tipped rod to find the location of a connected receptor that generates spikes. By pressing the skin with a glass rod with a blunt tip, we found a receptive field that fired spikes through the attached A-fiber. The spikes were visually inspected to determine whether their waveforms were consistent. After the recording, we loaded all waveforms and manually sorted spikes to remove noise that exhibited waveforms different from the target action potentials. We used isolated single-unit responses during the stimulation period for the analysis.

Mechanical stimulator

Axial indentation by the mechanical stimulator was driven by an actuator (Friedrich-Alexander Univ., Erlangen, Germany) controlled with a sinusoidal half-wave electric command signal. A load cell was attached to the mechanical stimulator's distal side of the metal shaft to measure the stimulus pressure. A magnet connected a cylindrical tip (diameter: 1 mm) to the bottom of the load cell. During the experiment, the tip was adjusted with a three-dimensional manipulator (U-3C, Narishige Co. ltd., Tokyo, Japan) and placed on the receptive field. The output voltage from the load cell was amplified (GSV-11 L, ME-Meßsysteme GmbH., Henningsdorf, Germany), digitized at 10 kHz, and stored in a computer. This data was used for proportional integral-derivative control to maintain accurate pressure. Manual calibration of the stimulator was performed by pressing the tip of the stimulator on a fine balance (AR 2140, Ohaus Corp., Parsippany, NJ, USA) and recording the actuator voltages at weights from 1 g to 50 g.

Modeling SA-I firings using interspike intervals

In a previous study, we developed a computational model to describe the spiking activity of SA-1 afferents in response to tactile pressure stimulations [8]. This model characterized the temporal structure of the interspike intervals (ISIs) of SA-1 afferents under different pressure stimulus intensities using a monotonically increasing polynomial function. The regression line was used to estimate the mean of a gamma distribution with a fixed variance, which was then used to extract a simulated ISI sequence that stochastically generated a train of spikes over time. More details about this model can be found in the study by Chun et al. [8].

Izhikevich biological neuron model

The Izhikevich model is a simple and widely used model for simulating the firings of biological neurons. It consists of a set of differential equations that describe the dynamics of the membrane potential ($v(t)$) and the adaptation variable ($u(t)$) in response to an input current ($I(t)$) (eq. (1)). The dynamics of the adaptation variable ($u(t)$) governed by its parameters (a and b) can illustrate the adaptation property of an artificial neuron (eq. (2)). The parameter a determines the time scale of u. In contrast, the parameter b determines the sensitivity of u to the membrane potential v. For example, if a is set to a small value, u will change slowly over time, resulting in a slower adaptation. On the other hand, if a is set to a larger value, u will change more quickly, resulting in a faster adaptation.

$$\frac{dv(t)}{dt}=Av(t)^2+Bv(t)+C-u(t)+I_{input}(t) \quad (1)$$

$$\frac{du(t)}{dt}=a(bv(t)-u(t)) \quad (2)$$

$$\text{if, } v(t)\geq 30 \text{ mV, then } \begin{cases} v(t)\leftarrow c \\ u(t)\leftarrow u(t)+d \end{cases} \quad (3)$$

In this study, we employ Euler's method in the simulation of the Izhikevich model with the initial values for v and u set to -70 mV and -14, respectively, as suggested by previous literature [33]. Euler's method is a first-order numerical method for solving ordinary differential equations (ODEs) [41]. Euler's method is relatively simple to implement and can solve linear and nonlinear ODEs, but its accuracy is limited for certain types of problems. To accurately simulate the dynamics of the Izhikevich model, it is essential to consider the integration period over which it is updated and stepped through. To match the data sampling rate of the animal studies, we set the integration period to 984 ms in this study. By fine-tuning the values of the parameters, we can modulate the model's overall dynamics. In particular, we set the parameters of the Izhikevich model to implement spike frequency adaptation (see Table 1) [42].

The parameter *a* in the Izhikevich model controls a time scale of the recovery variable *u*, which determines the rate at which *u* changes after a spike. A smaller value of *a* corresponds to a slower change in *u*, while a larger value of *a* corresponds to a faster change in *u*. The value of parameter *a* can significantly influence the dynamics of the Izhikevich model, such as the spike frequency, the duration of the spike, and the spike shape. In general, a smaller value of *a* results in a more tonic firing pattern, while a larger value of it leads to a more phasic firing pattern. The value of parameter *a* can be adjusted to replicate the firing patterns of different types of neurons.

Simulation results in Fig. 1 demonstrate that the interspike interval (ISI) decreases as the value of *a* increases, indicating that the model is firing at a higher rate (Fig. 1A, B). The mean firing rate is also shown to increase with increasing *a* (Fig. 1C). In addition, the effects of varying *a* on the membrane potential, recovery variable, and *v*-*u* phase plane are shown over time (Fig. 1D). The curve on the *v*-*u* phase plane becomes more tightly bound as the value of *a* increases. These simulation results suggest that parameter *a* plays a vital part in the dynamics of the Izhikevich model and can be used to fine-tune its behavior.

Table 1. Parameters of the spike frequency adaptation Izhikevich model used in this study

A	B	C
$0.04\ \frac{1}{\text{mV}\cdot\text{ms}}$	$5\ \frac{1}{\text{ms}}$	$140\ \frac{\text{mV}}{\text{ms}}$
a	**b**	**c**	**d**
0.01	0.2	-65 mV	8

Long-term adapting Izhikevich model

The conventional Izhikevich model exhibits spike frequency adaptation for a limited time, typically less than 1,000 ms. However, when the tactile nervous system receives sustained pressure stimulation for nearly 20 s, the SA-I afferent responses adapt over a more extended period, exceeding 1-second. To capture this long-term adaptation, we modify the Izhikevich model by progressively declining the parameter a, which represents the time scale of adaptation, whenever a spike occurs (eq. (6)). Our modified model, referred to as the long-term adapting Izhikevich model, can mimic the long-term adaptation of biological SA-I afferents in response to sustained stimuli, using the initial values for *v* and *u* as previously mentioned [33]. The following equations describe the dynamics of the long-term adapting Izhikevich model:

$$\frac{dv(t)}{dt}=Av(t)^2+Bv(t)+C-u(t)+S_pI_{input}(t) \quad (4)$$

$$\frac{du(t)}{dt}=a(t)(bv(t)-u(t)) \quad (5)$$

$$\text{if, } v(t)\geq 30 \text{ mV, then } \begin{cases} v(t)\leftarrow c \\ u(t)\leftarrow u(t)+d \\ a(t)\leftarrow a(t)/D_p \end{cases} \quad (6)$$

The proposed model introduces two new parameters: 1) a parameter S_p adjusts the magnitude of the injected current into the artificial neuron to match the peak firing rate of the artificial neuron with that of the biological SA-1 afferent neuron; and 2) the parameter D_p enables the progressive decrease of the parameter a, which modulates the recovery of membrane potentials. To find the optimal values of S_p and D_p that best match the spike patterns of biological SA-I afferents, we use a grid search scheme as follows:

1) For each of 30 SA-I afferent spike trains (6 stimulus intensities in 5 neurons), we estimate the firing rates over a 20 s stimulation period using bin counts with a time step of 10 ms and a bin width of 100 ms. Then, we fit an exponential function to the estimated time-varying firing rate to capture a slow decrease in the firing rate during stimulation. The exponential function is given by:

$$y(t)=\alpha\cdot exp(-\beta\cdot t) \quad (7)$$

Where $y(t)$ denotes a firing rate, t denotes time, and α and β are the parameters of the exponential function. As a result, we obtain 30 parameter sets, $\{\alpha_{c,p}\ \beta_{c,p}\}, c=1,\ldots,5, p=1,\ldots,6$, for the c-th neuron and the p-the stimulation intensity.

2) By sweeping all possible combinations of the values of $\{S_{c,p}\ D_{c,p}\}$, where $S_{c,p}$ spans from 0 to 200 with an increment of 1 and $D_{c,p}$ spans from 1 to 1.2 with an increment of 0.0001, we generate spike trains

https://doi.org/10.5607/en23005

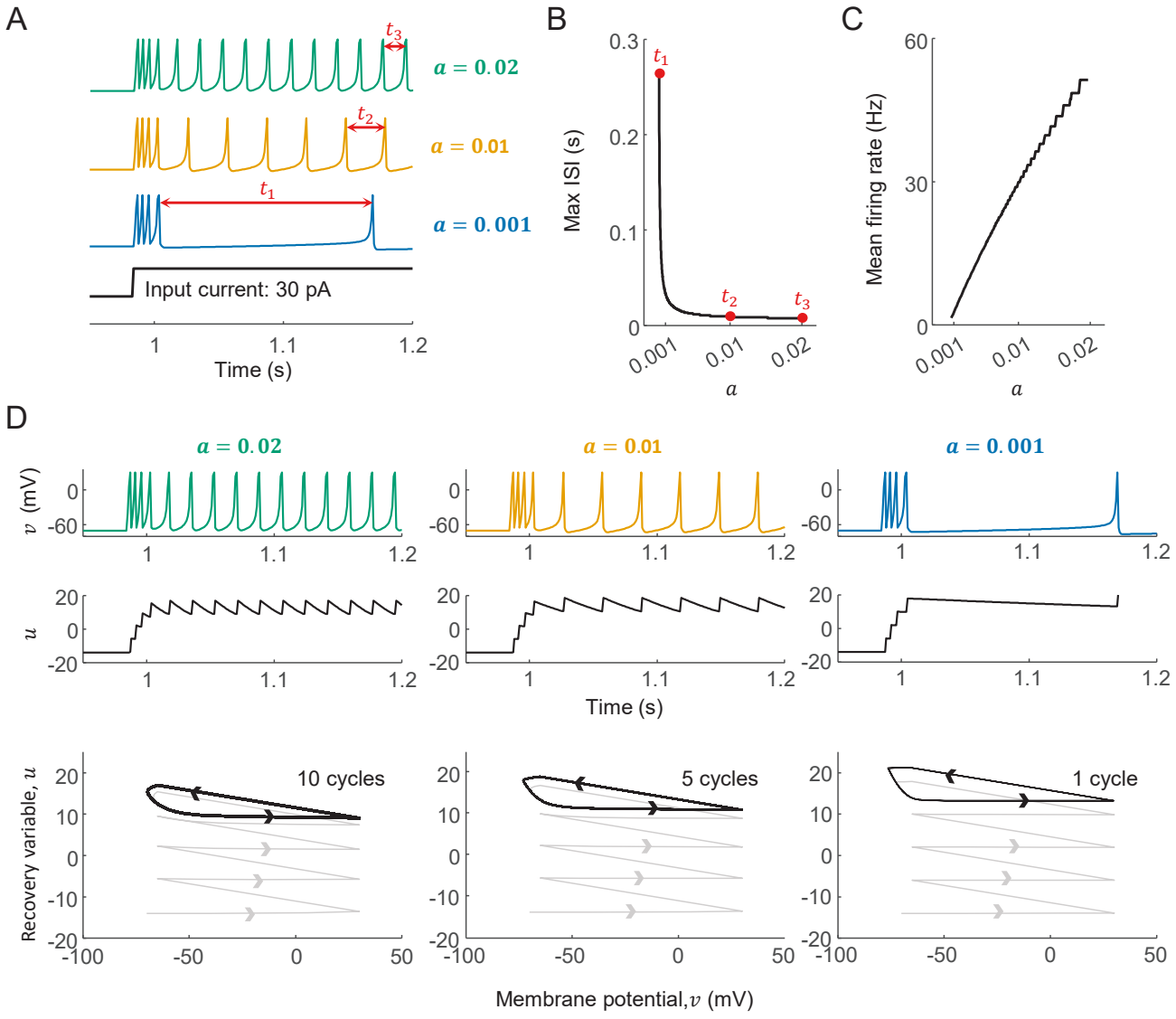

Fig. 1. The effects of the parameter *a* on the dynamics of the Izhikevich model under an input current of 30 pA. (A) Membrane potential over time with different values of *a* in the Izhikevich model. (B) The effects of parameter *a* on adapted interspike interval during continuous stimulation. (C) The effects of parameter *a* on mean firing rate during continuous stimulation. (D) The effects of parameter *a* on membrane potential (v), recovery variable (u), and v–u phase plane over time in the Izhikevich model.

using the long-term adaptation Izhikevich model. The generated spike train is converted to a firing rate in the same way as above. An exponential function is fitted to this firing rate to yield the estimates of parameters: $\{\hat{a}_{c,p}\ \hat{\beta}_{c,p}\}$. For each c and p, we find $\{\hat{a}_{c,p}\ \hat{\beta}_{c,p}\}$ from all possible combinations of the values of $\{S_{c,p}\ D_{c,p}\}$ that is closest to $\{a_{c,p}\ \beta_{c,p}\}$ found in 1).

3) From 2), we estimate optimal sets of $\{S_{c,p}\ D_{c,p}\}$ for c=1,…,5, p=1,…,6, and average over the neurons to obtain the parameters.

4) We use the sets of $\{S_p\ D_p\}$ for p=1,…,6 to generate spike trains with the long-term adaptation Izhikevich model.

Evaluating the similarity between model and biological spike trains

We use a spike distance metric to evaluate how close the models generate a spike train to that of biological SA-I afferents. The spike distance is calculated using Earth Mover's Distance (EMD), a measure of the shortest distance between two spike trains obtained by shifting a fraction of spikes from one train to the other [43]. A smaller spike distance indicates that the spike train generated by the model is closer to its biological counterpart.

RESULTS

Firing patterns of SA-I afferent

Using animal subjects, we analyzed the firing patterns of five SA-I afferent neurons in response to six different pressure intensities (0.1 mN~300 mN; Fig. 2A). Most firing rates followed an exponential curve that gradually decreased over the stimulation period (Fig. 2B, C). When relating the overall spike count during a 20 s stimulation period to the applied pressure, we observed that the average firing rate of each neuron increased progressively as the pressure increased from 0.1 mN to 50 mN and decreased back after 50 mN with only a few spikes observed at a pressure of 300 mN (Fig. 2D). We also investigated firing rates for each pressure intensity by normalizing the firing rates of each neuron for a given pressure and averaging them over neurons. Normalization was performed by $fr_{norm}=(fr-fr_{min})/(fr_{max}-fr_{min})$, where fr is a raw firing rate and fr_{max} and fr_{min} are the maximum and minimum firing rates, respectively. We observed that spike frequency adaptation occurred over several seconds in response to all pressure intensities (Fig. 2E). The time constant τ of exponential curves fitted to spike frequency adaptation was (4.70±1.54) s on average across pressure intensities. To analyze the decrease in firing rates over the long-term period, we identified the peak firing rate as the maximum firing rate over a 20 s sustained stimulation period. We then determined the time point at which the absolute gradient value of the exponential decay dropped below 1, which marked the beginning of the steady-state period. The steady-state firing rate was defined as the mean firing rate during this steady-state period. This allowed us to identify the point at which the firing rate had stabilized following a long adaptation period. By comparing the peak and steady-state firing rates, we could quantify changes in firing patterns that occurred over the sustained stimulation period. Our results showed a clear difference between the peak and steady-state firing rates for every pressure intensity (Fig. 2F).

Simulation of the vanilla Izhikevich model

We tested the conventional vanilla Izhikevich model with parameter sets used to implement spike frequency adaptation. Two sets of parameters were tested, one with original spike frequency adaptation and the other with a modified version of spike frequency adaptation by decreasing the parameter a further (Table 2). The Izhikevich model generated the spike train in response to a 100 pA input current. From the generated spike train, a firing rate was estimated with a time step of 10 ms and a bin width of 100 ms. Modified spike frequency adaptation by decreasing a further lowered the total spike count and increased the difference between the peak and the steady-state firing rates compared to the original spike frequency adaptation (Fig. 3). However, spike frequency adaptation by decreasing a only affected the firing rate right after adaptation but did not reveal long-term adaptation for longer period of time. Thus, simply changing the parameters of the vanilla Izhikevich model was not suitable for obtaining long-term spike frequency adaptation for SA-I afferents.

Simulating the dynamics of long-term spike frequency adaptation in SA-I neurons

Our simulation result indicated that the inhibition of sustained membrane recovery through the control of parameter a in the Izhikevich model did not lead to spike patterns that resembled those observed in biological SA-I afferent neurons (see Fig. 3). Additionally, inhibiting sustained membrane recovery did not significantly influence the duration of adaptation. However, our experimental data indicate that the SA-I afferent neurons exhibited stabilization following a long adaptation to sustained pressure. To model the dynamics of long-term spike frequency adaptation in SA-I afferent neurons, we modified the Izhikevich model with the decay parameters D_p and input scaler S_p and conducted a simulation to evaluate their impact on long-term adaptation.

The proposed long-term spike frequency adapting the Izhikevich model gradually decreased the parameter a, which inhibits membrane recovery, whenever a spike occurred. As a result, ISI also increased gradually. This allows for the implementation of spike frequency adaptation with a much slower time constant, enabling the creation of spike patterns with adaptation durations of several seconds, as demonstrated in Fig. 4. Through the simulation, we were able to determine the effect of altering the decay parameter D_p, specifically by incrementing it from 1 to 1.2 while maintaining a fixed input scaler S_p (Fig. 4A). Under the vanilla Izhikevich model, we observed that when parameter a did not decay (D_p=1), the spike frequency stabilized after a short period of adaptation lasting approximately 100 ms (Fig. 4B). An increase in the decay parameter from 1 to 1.2 resulted in a decrease in both the peak firing rates and the mean firing rate (Fig. 4C). The peak firing rate represents the highest frequency of firing during a specific time interval, while the mean firing rate is the average frequency of firing over that same interval. It is important to examine both the peak firing rates and mean firing rates due to the inherent nature of long-term adaptation, which leads to a distinction between these two metrics. Our goal is to demonstrate the differences between the peak and mean firing rates as they relate to the decay parameter or the Izhikevich input scaler. This analysis is crucial for providing a comprehensive understanding of the model's behavior in the context of our study. As the decay parameter was incrementally increased within a specific range, there was a corresponding

https://doi.org/10.5607/en23005

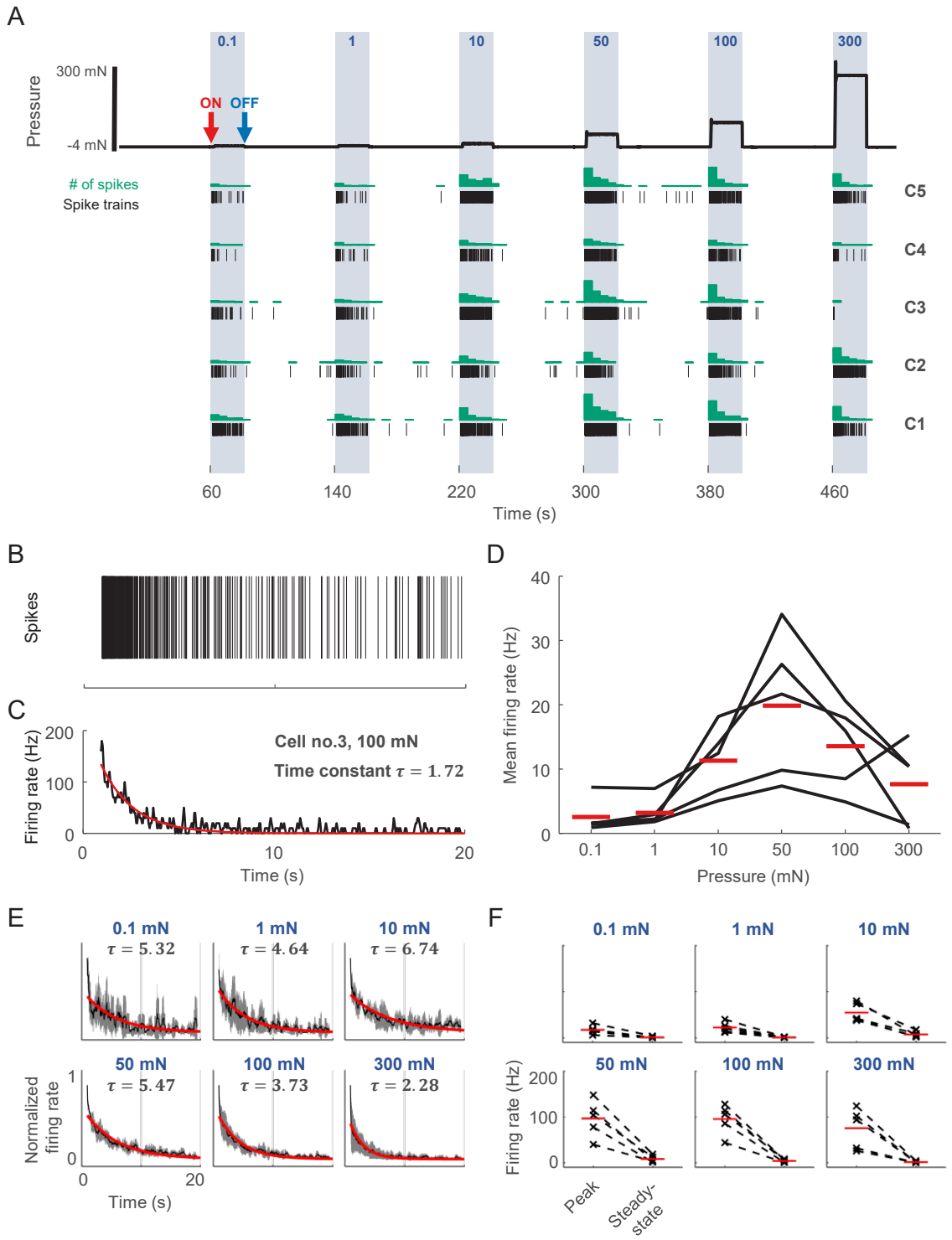

Fig. 2. Firing patterns of SA-I afferent neurons from ex vivo recordings. (A) The pressure stimulation (red line) and the spike response of five different SA-I afferent neurons (C1 to C5) were obtained from the ex-vivo experiment. The pressure intensity varies from 0.1 mN to 300 mN. Throughout the experiment, the stimulation periods are marked by a shaded background, each of which spans 20 s. Blue bars indicate the firing rate estimated by spike counts in 5 s bin. Black lines indicate the occurrence of spikes. The onset time of stimulations is marked. (B) The spike train of a representative neuron (C3) in response to 100 mN pressure. (C) The firing rate from the spike train in (B). The time constant (τ=1.70 s) is estimated from an exponential curve fitted to the firing rate. (D) The mean firing rate of each neuron averaged over the entire stimulation period for each pressure intensity. The red lines indicate the average firing rate over neurons. (E) Normalized firing rates of each neuron are averaged for each pressure intensity (grey lines) to which an exponential curve is fitted (red lines). The time constant of exponential curves is noted. (F) Comparison of the peak and steady-state firing rates.

decrease in the time constant, resulting in a shorter duration of adaptation in the neuron's firing rate (Fig. 4D). This suggests that the decay parameter has a significant influence on the shaping of spike patterns and the adaptation dynamics of the neuron.

As for the input scaler, the spike pattern of the SA-I afferent neuron differed as the input scaler was changed from 0 to 200 while maintaining a fixed decay parameter to 1.01 (Fig. 4E). Specifically, peak firing rates increased as the input scaler increased (Fig. 4F). Mean firing rates also increased as the input scaler was incrementally increased (Fig. 4G). The input scaler also affected the time constant of adaptation, even when the decay parameter remained constant (Fig. 4H). As the input scaler incrementally increased from 20, 50, and 100, the time constant decreased to 10.88, 6.52, and 4.38, respectively. These results could provide insights into the roles of the decay parameter and the input scaler in shaping the dynamics of the SA-I neuron.

Table 2. Parameter for the vanilla Izhikevich model

Neuron type of Izhikevich model	a	b	c	d
Spike frequency adaptation (SFA)	0.01	0.2	-65 mV	8
Modified SFA	0.001	0.2	-65 mV	8

Optimization of parameters for long-term spike frequency adaptation Izhikevich neuron model

To optimize the parameters of the proposed long-term Spike Frequency Adaptation (SFA) Izhikevich neuron model based on the biological neural signals of rodent SA-I afferents, we utilized a total size of (200×2,000) simulated long-term SFA Izhikevich models as well as the experimental data of rodent SA-I afferents. We first calculated the Euclidean distance between the parameters fitted to the experimental data, $\{\alpha_p\ \beta_p\}$ and the simulated data points, $\{\hat{\alpha}_p\ \hat{\beta}_p\}$, in a three-dimensional space consisting of the axes of the decay parameter and the injected current S. The experimental parameters $\{\alpha_p\ \beta_p\}$ were obtained by inverting the exponential curve fitted to the firing rate of the rodent SA-I afferents, while the model parameters $\{\hat{\alpha}_p\ \hat{\beta}_p\}$ were obtained by inverting the exponential curve fitted to the firing rate of the long-term SFA Izhikevich model. We found the parameters, $\{\hat{\alpha}_p\ \hat{\beta}_p\}$, which minimized the distance to $\{\alpha_p\ \beta_p\}$ for each pressure and each of five biological SA-I afferent neurons.

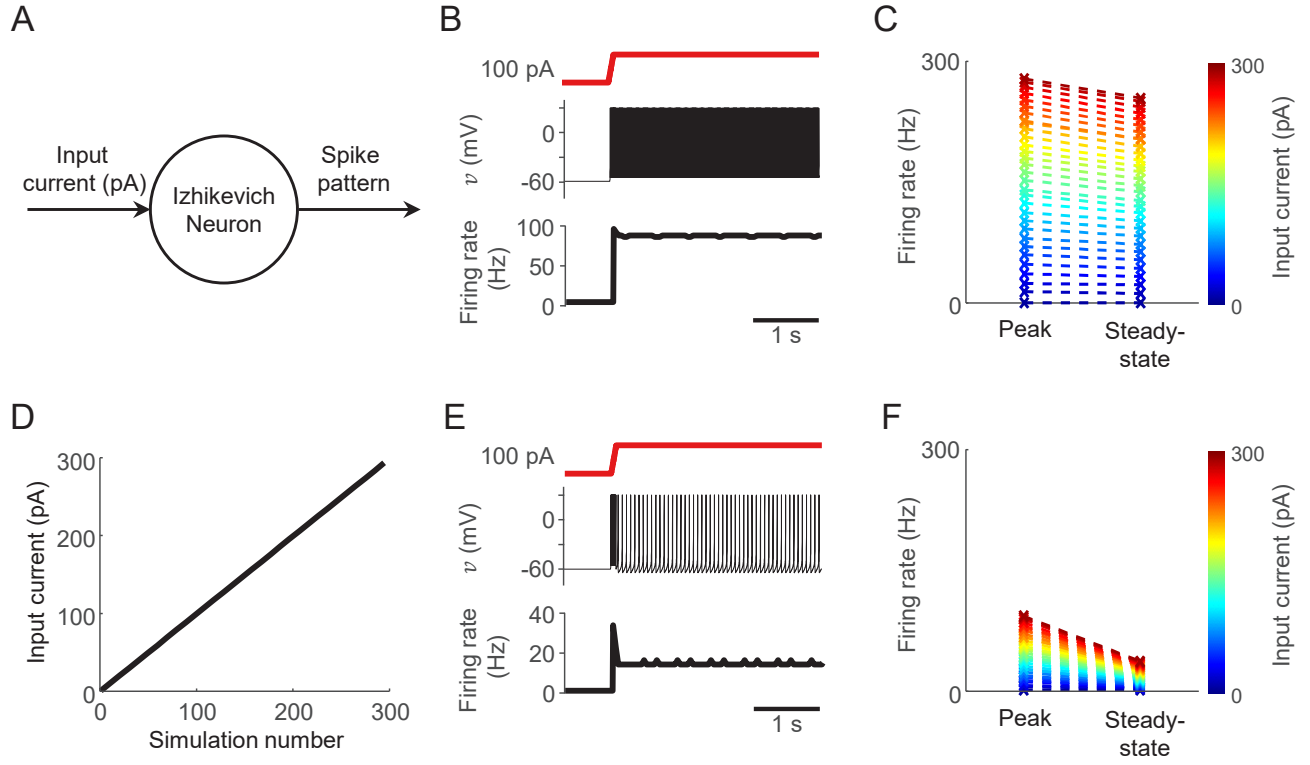

Fig. 3. Simulations of the vanilla Izhikevich models with different recovery time constant *a* values. (A) Schematic representation of input current driving an Izhikevich neuron model simulation to produce a spike pattern. (B) Representative spike train generation exhibiting original spike frequency adaptation in response to a 100 pA input current for 20 s, with the adaptation parameter *a* set to 0.01. (C) Peak and steady-state firing rates of spike trains depicted in (B). (D) The input current values ranging from 0 to 300 in increments of 1, used for driving the Izhikevich neuron model simulations. (E) Representative spike train generation with modified spike frequency adaptation, where the adaptation parameter *a* is set to 0.001. (F) Peak and steady-state firing rates of spike trains presented in (E).

https://doi.org/10.5607/en23005

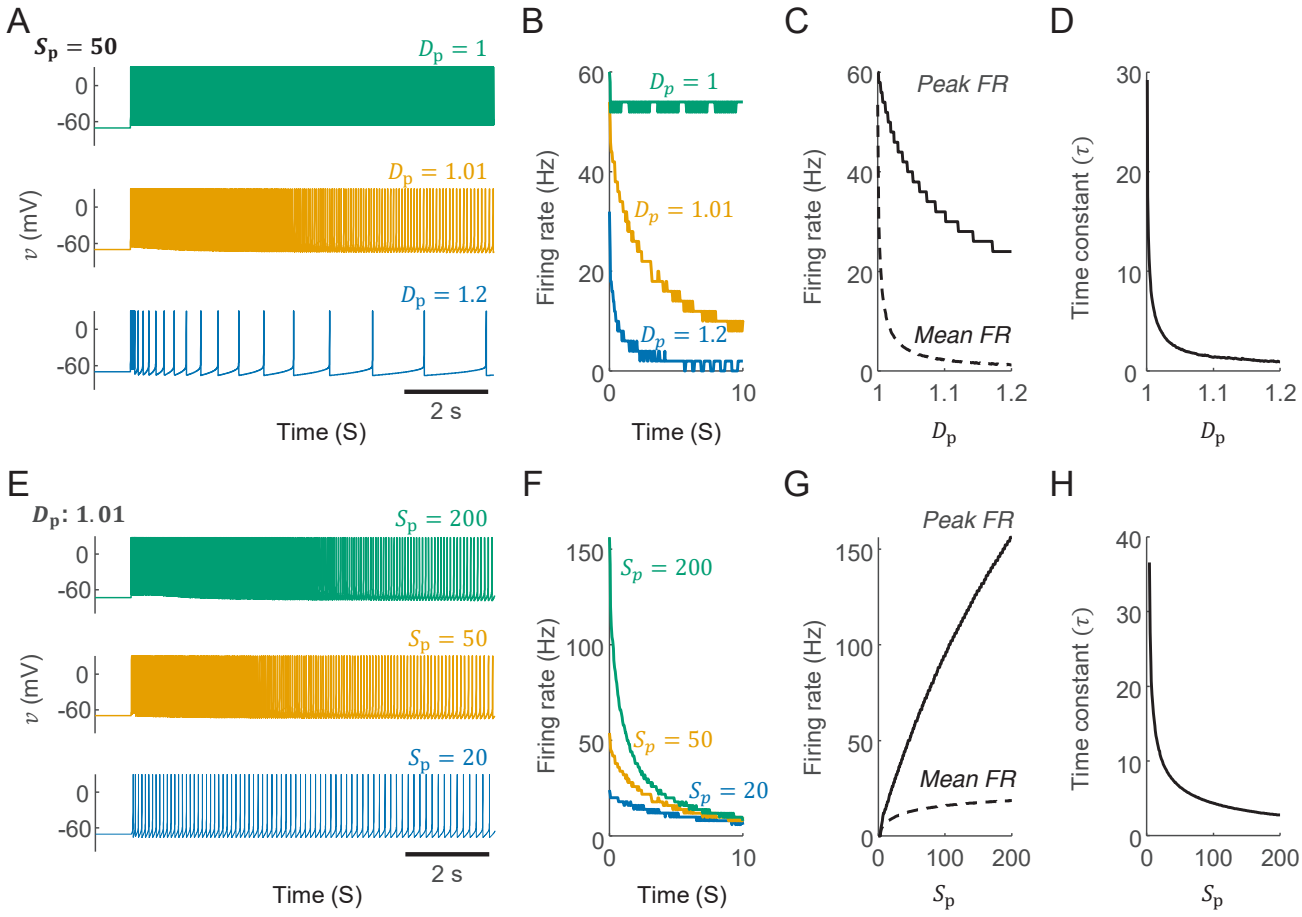

Fig. 4. Response pattern and firing rate in response to decay and input scale parameters of modified spike frequency adapting Izhikevich model. (A) The response pattern of modified spike frequency adaptive Izhikevich model in response to an input scaler fixed at 50 (Decay parameter D_p=1.2, 1.01, or 1). (B) Firing rate for three decay parameters with an input scaler fixed at 50. (C) The solid line represents the peak firing rate, and the dashed line represents the mean firing rate over the decay parameter D_p with an input scaler fixed at 50 for 20 seconds. (D) The time constant over the decay parameter D_p with an input scaler fixed at 50. (E) Spike train generation with modified spike frequency adaptive Izhikevich model in response to a decay parameter fixed at 1.01 (Input scaler S_p=20, 50, or 100). (F) Firing rate for three different input scalers with a decay parameter fixed at 1.01. (G) The solid line represents the peak firing rate, and the dashed line represents the mean firing rate of the firing rate over input scaler S_p with a decay parameter fixed at 1.01 for 20 seconds. (H) The time constant over the input scaler S_p with a decay parameter fixed at 1.01.

Then, we averaged these parameters across five SA-I afferent neurons. The simulation model parameters $\{S_p\ D_p\}$ with exponential parameters $\{\alpha_p\ \beta_p\}$ were chosen as the long-term SFA Izhikevich model corresponding to the appropriate pressure. The selected parameters of the long-term SFA Izhikevich model for each corresponding pressure are listed in Table 3.

Table 3. The optimal parameters of long-term spike frequency adaptation model for different sustained pressure

Pressure (mN)	Parameter	
	S_p	D_p
0.1	20.4	1.1094
1	21.4	1.0629
10	42	1.0153
50	85.6	1.0094
100	108	1.0154
300	105.6	1.0759

Performance of the long-term spike frequency adaptation Izhikevich

Spike trains generated by the long-term SFA Izhikevich model demonstrated spike frequency adaptation over several seconds similar to biological SA-I neurons for different input pressure intensities, while the vanilla SFA Izhikevich model and the ISI based spiking model did not reveal such long-term SFA (see representative examples in Fig. 5). We evaluated the degree of similarity between the spike trains generated by the model and those of bio-

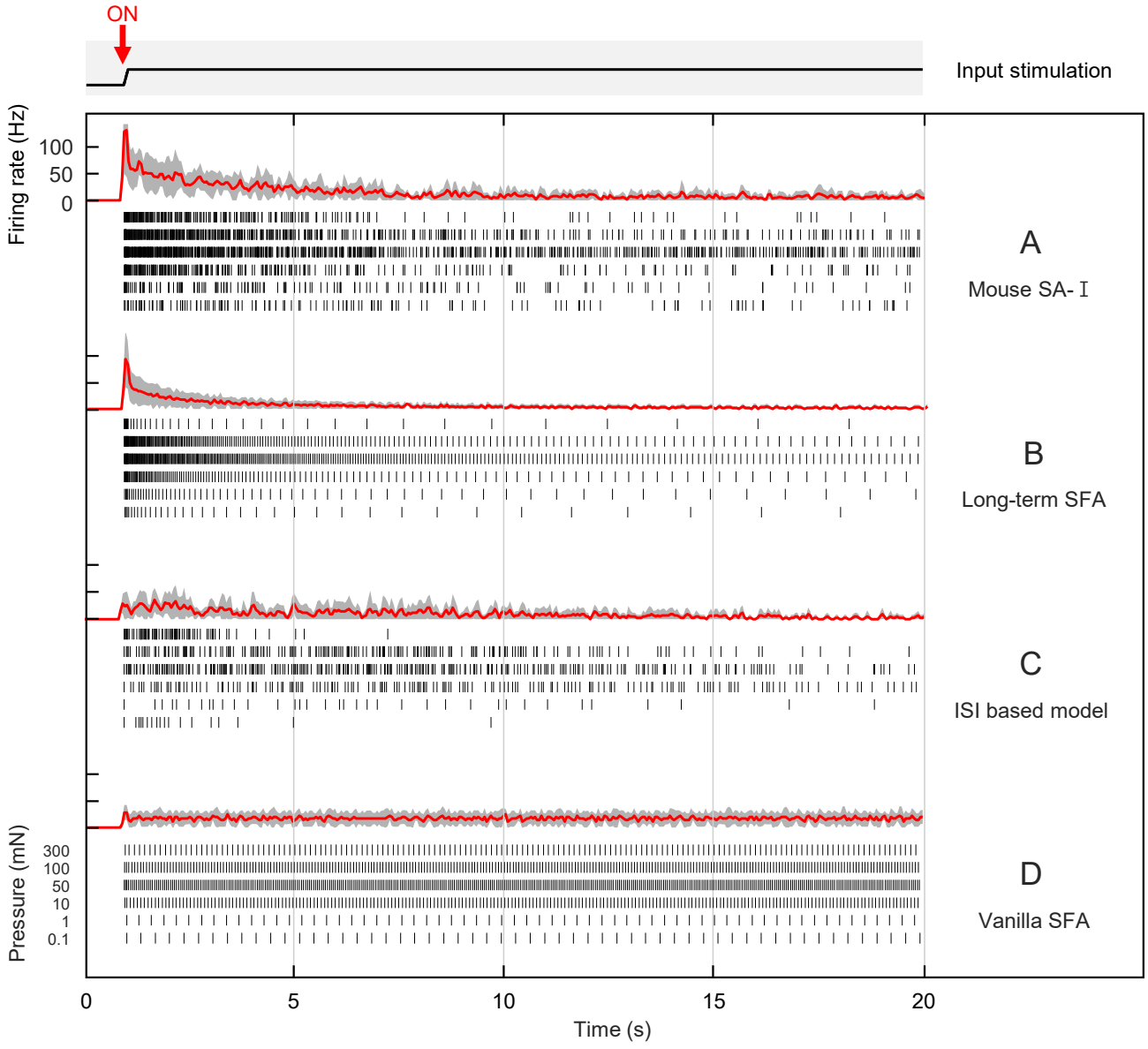

Fig. 5. Spike responses of (A) Mouse SA-I afferents, (B) Long-term SFA Izhikevich model, (C) ISI fitting model, and (D) Vanilla SFA Izhikevich model.

logical SA-I afferents using spike train distance measured by Earth Mover's Distance (EMD, [43]). A smaller spike distance indicates a closer match between the model's spike train and its biological counterpart. Our results showed that the long-term SFA Izhikevich model exhibited significantly smaller spike distance than other models ($p<0.01$, *t*-test) (Fig. 6A). Also, the difference between the peak and steady-state firing rates in the long-term SFA Izhikevich model was more similar to the biological data than other models (Fig. 6B).

DISCUSSION

We proposed a novel biological neuron model (BNM) for slowly adapting type 1 (SA-I) afferent neurons to develop a biomimetic artificial tactile sensing system that can detect sustained mechanical touch. We tested if the BNM, designed by modifying the Izhikevich model to incorporate long-term spike frequency adaptation, could accurately replicate the firing patterns of biological SA-I afferent neurons in response to sustained pressure. To test the validity of the BNM, we obtained firing data from ex vivo experiments on SA-I afferent neurons in rodents. We used this data to search for optimal parameter values for the BNM. We then gener-

 https://doi.org/10.5607/en23005

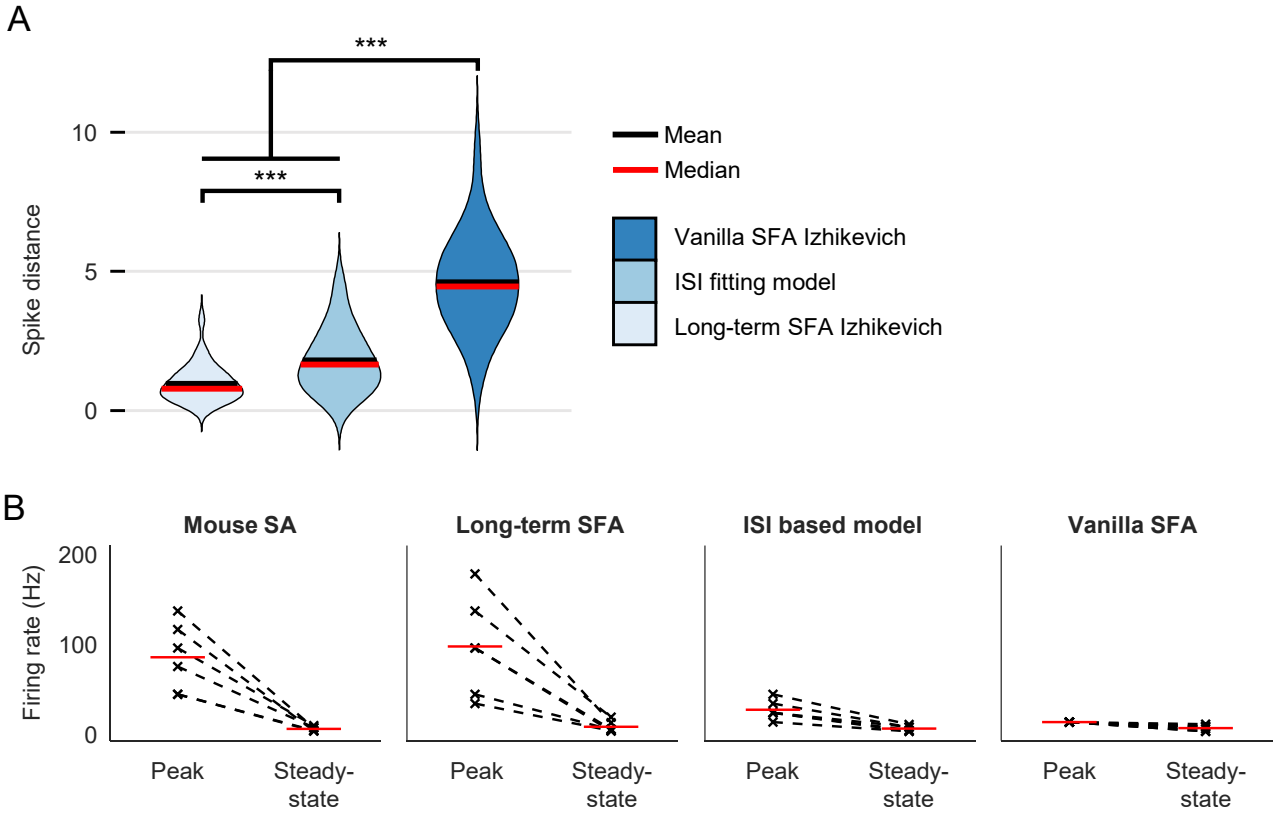

Fig. 6. Performance of the long-term spike frequency adaptation (SFA) Izhikevich model, the ISI fitting model, and the vanilla SFA Izhikevich model. (A) Violin plot of the spike distance between the spike trains of mouse SA-1 afferents and those generated by each model. (B) Comparison of the peak and steady-state firing rates between the three models (p values are significant according to the Student's *t*-test; ***p<0.001).

ated spike trains using the BNM and compared the resulting spike trains to those of the biological SA-I afferent neurons using spike distance metrics. Our results showed that the BNM could generate spike trains with long-term adaptation, which was not achievable with other conventional models. This suggests that the proposed BNM can simulate the dynamics of long-term spike frequency adaptation in SA-I afferent neurons. Remarkably, ex vivo firing data revealed that the intensity of applied pressure strongly influenced the firing patterns of SA-I afferent neurons. As the pressure increased from 0.1 mN to 50 mN, the average firing rate of each neuron progressively increased. This trend was reversed at higher pressure intensities, with a decrease in the average firing rate observed at a pressure of 300 mN. This suggests that the relationship between firing patterns of SA-I afferent neurons and pressure intensity may be nonlinear and highly sensitive to changes in pressure intensity. Nevertheless, a further rigorous experiment with a neurophysical model should follow to justify this tentative observation.

We found that spike frequency adaptation occurred over several seconds in response to all pressure intensities, as evidenced by the exponential decay in firing rate over time. The time constant of this decay was approximately 4.7-second on average across all pressure intensities. It would be interesting to see if such a time constant is biologically intrinsic or not; it is questionable whether the range of time constant remains unchanged if stimulation duration changes. Furthermore, we observed a significant difference between the peak and steady-state firing rates for every pressure intensity, indicating that the firing patterns of SA-I afferent neurons undergo substantial changes over extended periods in response to sustained pressure. Furthermore, our simulation results suggest that the long-term adapting Izhikevich model can capture the behavior of real biological SA-I afferent neurons that exhibit long-term adaptation. Additionally, we found that the decay parameter D_p and the input scaler S_p have a significant influence on the adaptation dynamics of the neuron, shaping the spike patterns and duration of adaptation.

One potential advantage of the long-term adapting Izhikevich model is that it can more accurately capture the behavior of real

biological neurons that exhibit long-term adaptation, such as SA-I afferent neurons. This can be useful for studying the function and role of similarly behaving neurons in the brain and for developing more realistic computational models of brain computation. The long-term SFA Izhikevich model may also offer novel ways of creating artificial neurons in spiking neural networks, which can be applied for image processing, artificial tactile sensing, and robotics. Future investigation of the benefits and limitations of the long-term SFA Izhikevich model in such applications may be of interest. In particular, the scalability of the long-term SFA Izhikevich model to other types of tactile afferents, such as RA (rapid adapting) afferents, may be worth exploring. The long-term SFA Izhikevich model may provide a more efficient and realistic approach to artificial tactile sensing technology by emphasizing the advantages in terms of power consumption and the requirement for sensory adaptation.

ACKNOWLEDGEMENTS

This study was supported by Brain Convergence Research Programs of the National Research Foundation (NRF-2019M3E5D2A01058328) funded by the Korean Government (MSIT) and the U-K (UNIST-Korea) research brand program (1.220032.01) funded by UNIST (Ulsan National Institute of Science & Technology).

REFERENCES

1. Wang X, Dong L, Zhang H, Yu R, Pan C, Wang ZL (2015) Recent progress in electronic skin. Adv Sci (Weinh) 2:1500169.
2. Cao HL, Cai SQ (2022) Recent advances in electronic skins: material progress and applications. Front Bioeng Biotechnol 10:1083579.
3. Wang C, Hwang D, Yu Z, Takei K, Park J, Chen T, Ma B, Javey A (2013) User-interactive electronic skin for instantaneous pressure visualization. Nat Mater 12:899-904.
4. Chun S, Kim DW, Baik S, Lee HJ, Lee JH, Bhang SH, Pang, C (2018) Conductive and stretchable adhesive electronics with miniaturized octopus-like suckers against dry/wet skin for biosignal monitoring. Adv Funct Mater 28:1805224.
5. Hou C, Wang H, Zhang Q, Li Y, Zhu M (2014) Highly conductive, flexible, and compressible all-graphene passive electronic skin for sensing human touch. Adv Mater 26:5018-5024.
6. Chortos A, Liu J, Bao Z (2016) Pursuing prosthetic electronic skin. Nat Mater 15:937-950.
7. Gerratt AP, Michaud HO, Lacour SP (2015) Elastomeric electronic skin for prosthetic tactile sensation. Adv Funct Mater 25:2287-2295.
8. Chun S, Kim JS, Yoo Y, Choi Y, Jung SJ, Jang D, Lee G, Song KI, Nam KS, Youn I, Son D, Pang C, Jeong Y, Jung H, Kim YJ, Choi BD, Kim J, Kim SP, Park W, Park S (2021) An artificial neural tactile sensing system. Nat Electron 4:429-438.
9. Park J, Kim M, Lee Y, Lee HS, Ko H (2015) Fingertip skin-inspired microstructured ferroelectric skins discriminate static/dynamic pressure and temperature stimuli. Sci Adv 1:e1500661.
10. Tee BC, Chortos A, Berndt A, Nguyen AK, Tom A, McGuire A, Lin ZC, Tien K, Bae WG, Wang H, Mei P, Chou HH, Cui B, Deisseroth K, Ng TN, Bao Z (2015) A skin-inspired organic digital mechanoreceptor. Science 350:313-316.
11. Ha M, Park J, Lee Y, Ko H (2015) Triboelectric generators and sensors for self-powered wearable electronics. ACS Nano 9:3421-3427.
12. Núñez CG, Navaraj WT, Polat EO, Dahiya R (2017) Energy-autonomous, flexible, and transparent tactile skin. Adv Funct Mater 27:1606287.
13. Kim SY, Park S, Park HW, Park DH, Jeong Y, Kim DH (2015) Highly sensitive and multimodal all-carbon skin sensors capable of simultaneously detecting tactile and biological stimuli. Adv Mater 27:4178-4185.
14. Jin ML, Park S, Lee Y, Lee JH, Chung J, Kim JS, Kim JS, Kim SY, Jee E, Kim DW, Chung JW, Lee SG, Choi D, Jung HT, Kim DH (2017) An ultrasensitive, visco-poroelastic artificial mechanotransducer skin inspired by Piezo2 protein in mammalian merkel cells. Adv Mater 29:1605973.
15. Schwartz G, Tee BC, Mei J, Appleton AL, Kim DH, Wang H, Bao Z (2013) Flexible polymer transistors with high pressure sensitivity for application in electronic skin and health monitoring. Nat Commun 4:1859.
16. Lee WW, Tan YJ, Yao H, Li S, See HH, Hon M, Ng KA, Xiong B, Ho JS, Tee BCK (2019) A neuro-inspired artificial peripheral nervous system for scalable electronic skins. Sci Robot 4:eaax2198.
17. Chi C, Sun X, Xue N, Li T, Liu C (2018) Recent progress in technologies for tactile sensors. Sensors (Basel) 18:948.
18. Wu Y, Liu Y, Zhou Y, Man Q, Hu C, Asghar W, Li F, Yu Z, Shang J, Liu G, Liao M, Li RW (2018) A skin-inspired tactile sensor for smart prosthetics. Sci Robot 3:eaat0429.
19. Williams I, Constandinou T (2013) An energy-efficient, dynamic voltage scaling neural stimulator for a proprioceptive prosthesis. IEEE Trans Biomed Circuits Syst 7:129-139.
20. Lucarotti C, Oddo CM, Vitiello N, Carrozza MC (2013) Synthetic and bio-artificial tactile sensing: a review. Sensors (Basel) 13:1435-1466.
21. Drotlef DM, Amjadi M, Yunusa M, Sitti M (2017) Bioinspired

composite microfibers for skin adhesion and signal amplification of wearable sensors. Adv Mater 29:1701353.
22. Abraira VE, Ginty DD (2013) The sensory neurons of touch. Neuron 79:618-639.
23. Tiwana MI, Redmond SJ, Lovell NH (2012) A review of tactile sensing technologies with applications in biomedical engineering. Sens Actuators Phys 179:17-31.
24. Indiveri G, Linares-Barranco B, Hamilton TJ, van Schaik A, Etienne-Cummings R, Delbruck T, Liu SC, Dudek P, Häfliger P, Renaud S, Schemmel J, Cauwenberghs G, Arthur J, Hynna K, Folowosele F, Saighi S, Serrano-Gotarredona T, Wijekoon J, Wang Y, Boahen K (2011) Neuromorphic silicon neuron circuits. Front Neurosci 5:73.
25. Kim Y, Chortos A, Xu W, Liu Y, Oh JY, Son D, Kang J, Foudeh AM, Zhu C, Lee Y, Niu S, Liu J, Pfattner R, Bao Z, Lee TW (2018) A bioinspired flexible organic artificial afferent nerve. Science 360:998-1003.
26. Vallbo AB, Johansson RS (1984) Properties of cutaneous mechanoreceptors in the human hand related to touch sensation. Hum Neurobiol 3:3-14.
27. Johnson KO, Hsiao SS (1992) Neural mechanisms of tactual form and texture perception. Annu Rev Neurosci 15:227-250.
28. Gong S, Schwalb W, Wang Y, Chen Y, Tang Y, Si J, Shirinzadeh B, Cheng W (2014) A wearable and highly sensitive pressure sensor with ultrathin gold nanowires. Nat Commun 5:3132.
29. Salimi-Nezhad N, Ilbeigi E, Amiri M, Falotico E, Laschi C (2020) A digital hardware system for spiking network of tactile afferents. Front Neurosci 13:1330.
30. Hodgkin AL, Huxley AF (1952) A quantitative description of membrane current and its application to conduction and excitation in nerve. J Physiol 117:500-544.
31. Burkitt AN (2006) A review of the integrate-and-fire neuron model: I. Homogeneous synaptic input. Biol Cybern 95:1-19.
32. Heiberg T, Kriener B, Tetzlaff T, Einevoll GT, Plesser HE (2018) Firing-rate models for neurons with a broad repertoire of spiking behaviors. J Comput Neurosci 45:103-132.
33. Izhikevich EM (2003) Simple model of spiking neurons. IEEE Trans Neural Netw 14:1569-1572.
34. Gunasekaran H, Spigler G, Mazzoni A, Cataldo E, Oddo CM (2019) Convergence of regular spiking and intrinsically bursting Izhikevich neuron models as a function of discretization time with Euler method. Neurocomputing 350:237-247.
35. Parvizi-Fard A, Amiri M, Kumar D, Iskarous MM, Thakor NV (2021) A functional spiking neuronal network for tactile sensing pathway to process edge orientation. Sci Rep 11:1320.
36. Izhikevich EM (2004) Which model to use for cortical spiking neurons? IEEE Trans Neural Netw 15:1063-1070.
37. Pozzorini C, Naud R, Mensi S, Gerstner W (2013) Temporal whitening by power-law adaptation in neocortical neurons. Nat Neurosci 16:942-948.
38. Guan D, Armstrong WE, Foehring RC (2015) Electrophysiological properties of genetically identified subtypes of layer 5 neocortical pyramidal neurons: Ca^{2+} dependence and differential modulation by norepinephrine. J Neurophysiol 113:2014-2032.
39. Liu YH, Wang XJ (2001) Spike-frequency adaptation of a generalized leaky integrate-and-fire model neuron. J Comput Neurosci 10:25-45.
40. Höger U, French AS (2005) Slow adaptation in spider mechanoreceptor neurons. J Comp Physiol A Neuroethol Sens Neural Behav Physiol 191:403-411.
41. Butcher JC (2016) Numerical methods for ordinary differential equations. John Wiley & Sons, Chichester.
42. Esposito D, Lanotte F, Mugnai C, Massari L, Camboni D, Mazzoni A, Oddo CM (2019) A neuromorphic model to match the spiking activity of merkel mechanoreceptors with biomimetic tactile sensors for bioengineering applications. IEEE Trans Med Robot Bionics 1:97-105.
43. Sihn D, Kim SP (2019) A spike train distance robust to firing rate changes based on the earth mover's distance. Front Comput Neurosci 13:82.